Development and optimization of an ocular hydrogel adhesive patch using definitive screening design (DSD)

Journal:	*Biomaterials Science*
Manuscript ID	BM-ART-06-2022-001013.R1
Article Type:	Paper
Date Submitted by the Author:	27-Sep-2022
Complete List of Authors:	Gholizdeh, Shima; UCLA, Chemical and Biomolecular Engineering Chen, Xi; UCLA, Chemical and Biomolecular Engineering Yung, Ann; Schepens Eye Research Institute of Massachusetts Eye and Ear, Ophthalmology Naderi, Amirreza; Harvard Medical School Ghovvati, Mahsa; UCLA, Chemical and Biomolecular engineering Liu, Yangcheng; UCLA Farzad, Ashkan; Sanquin product support and development Mostafavi, Azadeh; UCLA Dana, Reza; Schepens Eye Research Institute of Massachusetts Eye and Ear, Annabi, Nasim; UCLA, Chemical and Biomolecular Engineering

SCHOLARONE™
Manuscripts

ARTICLE

Development and optimization of an ocular hydrogel adhesive patch using definitive screening design (DSD)

Shima Gholizadeh[1], Xi Chen[1], Ann Yung[2], Amirreza Naderi[2], Mahsa Ghovvati[1], Yangcheng Liu[1], Ashkan Farzad[3], Azadeh Mostafavi[1], Reza Dana[2], Nasim Annabi[1]

Adhesive hydrogels based on chemically modified photocrosslinkable polymers with specific physicochemical properties are frequently utilized for sealing wounds or incisions. These adhesive hydrogels offer tunable characteristics such as tailorable tissue adhesion, mechanical properties, swelling characteristics, and enzymatic degradability. In this study, we developed and optimized a photocrosslinkable adhesive patch, GelPatch, with high burst pressure, minimal swelling, and specific mechanical properties for application as an ocular (sclera and subconjuctical) tissue adhesive. To achieve this, we formulated a series of hydrogel patches composed of different polymers with various levels of methacrylation, molecular weights, and hydrophobic/hydrophilic properties. A computerized multifactorial definitive screening design (DSD) analysis was performed to identify the most prominent components impacting critical response parameters such as adhesion, swelling ratio, elastic modulus, and second order interactions between applied components. These parameters were mathematically processed to generate a predictive model that identifies the linear and non-linear correlations between these factors. In conclusion, an optimized formulation of GelPatch was selected based on two modified polymers: gelatin methacryloyl (GelMA) and glycidyl methacrylated hyaluronic acid (HAGM). The *ex vivo* results confirmed adhesion and retention of the optimized hydrogel subconjunctivally and on the sclera for up to 4 days. The developed formulation has potential to be used as an ocular sealant for quick repair of laceration type ocular injuries.

Keywords: Ocular adhesive, ocular sealant, Design of Experiment (DoE), Definitive screening design (DSD)

Introduction

With almost 2.5 million new cases each year in the United States, ocular injuries represent a major burden for patients and healthcare providers[1]. Ocular injuries can induce chronic inflammation and consequentially result in scarring, causing corneal opacities, one of the leading causes of vision impairment worldwide[2]. Injuries to the eye are particularly challenging due to disruption of the ocular protective barriers and thus, compromising the eye's integrity[3-5].

Moreover, ocular injuries that involve foreign bodies or post-surgical care usually require complicated therapeutic regimens with high frequency of application. This can result in medical complications and a decrease in therapeutic efficacy, particularly among the elderly population, due to lack of compliance[6].

Thus far, there are several types of ocular adhesives developed with the primary purpose of sealing ocular injuries. McTiernan *et al.* has developed an adhesive composed of short collagen like peptides and an 8-arm maleimide modified polyethylenglycol (PEG) suitable for application as a sealant for use in corneal transplantation[7]. Although the developed hydrogel showed a burst pressure of ~20 kPa when applied on *ex vivo* porcine corneas, no data on its swelling properties was reported. Additionally, the engineered hydrogel was stiff (elastic modulus ~160 kPa) with limited elasticity. PEG-based ocular sealants have been used as an adhesive for sealing small surface areas (i.e., microincisions); however, they generally require multicomponent mixing and suffer from short application windows[8]. One example is ReSure® (Ocular Therapeutix Inc.) which requires two-component mixing of PEG and a trilysine acetate solution that only allows for a 20 second window of application before the initiation of polymerization[9, 10]. Fibrin-based glues (i.e., Evicel®, Tisseel® and Artiss®), composed of human fibrinogen and human thrombin, are packaged separately, and polymerize once mixed together[11]. Due to their biological origin, fibrin glues are more biocompatible and well-tolerated by the body, including the eye, as compared to cyanoacrylate glues[12]. However, their adhesive strength is relatively lower and requires longer polymerization times (~20 min)[11, 13]. Therefore, fibrin glues are not ideal for ocular applications and are instead used off-label in cases such as securing the amniotic membrane in place during graft transplatation[14].

[1] *Chemical and Biomolecular Engineering Department, University of California - Los Angeles, Los Angeles, CA, USA.*
[2] *Schepens Eye Research Institute, Mass Eye and Ear, Harvard Medical School, Department of Ophthalmology, Boston, MA, USA.*
[3] *Sanquin product support and development, Sanquin plasma products B.V., Amsterdam, The Netherlands.*

Our team has previously developed a naturally derived adhesive hydrogel for corneal tissue regeneration, named GelCORE, based on gelatin methacryloyl (GelMA)[13]. Although the GelCORE adhesive showed high biocompatibility and partial adhesion to stromal defects on the cornea, its adhesion to intact corneal tissue was not studied. Additionally, GelCORE was not viscous enough to prevent substantial runoff before photopolymerization; therefore, it was not capable of sealing laceration defects with continuous leakage. To address this problem, we have recently developed an alternative hydrogel patch with a higher initial viscosity[15]. However, this formulation also suffered from excessive swelling and low burst pressure, which can reduce adhesion to the corneal tissue.

Therefore, to address the aforementioned limitations we applied a systematic approach to further optimize the properties of our ocular adhesive patch in order to enhance its adherence to the cornea, sclera, and subconjunctival space. Our optimized formulation in this study has the potential to quickly seal the wounded ocular area. The developed ocular adhesive patch, named GelPatch, can be easily applied to the sclera and subconjunctival tissues, and crosslinked via exposure to visible light to adhere to the underlying tissue **(Fig. 1A)**. First, we predefined the desired characteristics of the patch based on obtained results from previous studies in the liquid and solid states[13, 15]. The characteristics include: 1) high wet tissue retention upon instillation, 2) maximal tissue adhesion, 3) minimal swelling, and 4) optimized mechanical properties to minimize ocular sensation. Next, Design of Experiment (DoE) was applied as a tool to screen for these critical factors which impact the properties of the GelPatch. These factors are comprised of different types of photocurable polymers with varying degrees and types of functionalization. Finally, definitive screening design (DSD) was considered as a model to screen critical factors (i.e., polymer types, molecular weights, and concentrations) that had a significant impact on the response parameters such as burst pressure, swelling ratio, mechanical strength, and elasticity. In addition, utilization of DSD aided in a systematic selection of the most ideal formulation which can be used for ocular sealing.

Experimental section

Materials

Pluronic® F-127 (PL127), Tween 20, methacrylic anhydride triethanolamine (TEA), N-vinylcaprolactam (VC), Eosin Y disodium salt, and gelatin (porcine skin, gel strength: 300 Bloom, Type A) were purchased from Sigma Aldrich. Porcine gelatin (Instagel®) Bloom 225 was purchased from PB Leiner USA, Davenport. All solvents were analytical grade and supplied by Sigma Aldrich or Fisher Scientific. All cell culture materials were provided by Sigma Aldrich. PrestoBlue assay was obtained from Thermo Fisher Scientific. LIVE/DEAD kit was purchased from Invitrogen. Rabbit eyeballs were purchased from Sierra Medical.

Synthesis of gelatin methacryloyl (GelMA)

Two types of porcine gelatin (B300 and B225) were utilized for the synthesis of GelMA. Applied gelatin types were varied based on their molecular weight distributions. Gelatin B300 and B225 had molecular weight distribution of 80-100 kDa and 40-60 kDa, respectively. The methacrylation of the porcine gelatin was carried out based on previously reported methods[16]. Briefly, 10% (w/v) of gelatin from porcine skin (B300 or B225) was dissolved in Dulbecco's Phosphate-Buffered Saline (DPBS) and reacted with 8 mL of methacrylic anhydride (Sigma Aldrich) for 3.5 h at 60°C. The reaction was stopped by a two times dilution with DPBS and was dialyzed for 5 days to remove any unreacted methacrylic anhydride and placed at -80°C for 24 h. The frozen polymer was then freeze-dried for 5 days.

Synthesis of poly(ethylene glycol) diacrylate (PEGDA)

To synthesize PEGDA, poly(ethylene glycol) (PEG, 35 kDa, Sigma Aldrich) was chemically reacted with acryloyl chloride (Sigma Aldrich) based on a previously described method[17]. Briefly, 10 g of PEG was dissolved in 100 mL of dichloromethane (10% w/v) at 4°C. Next, triethylamine (Sigma Aldrich) was added to the PEG solution under a nitrogen environment. Then, 103.4 mg (11.4 mM) of acryloryl chloride (Sigma Aldrich) was added and dissolved in the PEG solution and stirred overnight under dry N_2 gas. The molar ratio of PEG, acryloyl chloride, and triethylamine was 1:4:4. Finally, the insoluble salt (triethylamine-HCl) was filtered (celite 545 powder and alumina column), and the product was precipitated by adding ice-cold ether. The crude product was filtered with a 9 μm paper filter and dried in a vacuum desiccator overnight to remove unreacted materials.

Synthesis of methacrylated hyaluronic acid (HAMA)

Hyaluronic acid (HA) was methacrylated as previously reported by Hachet *et al.* with minor adjustment[18]. Briefly, 5 g (12.5 mmol of disaccharide units) of HA was dissolved in 250 mL of ultrapure water and 250 mL of N, N-dimethylformamide (DMF). Next, dropwise addition of 5 mL of methacrylic anhydride (33.6 mmol) was done at 4°C while maintaining the pH between 8 and 9 with the addition of aqueous NaOH solution (0.5 M). The polymer mixture was then stirred overnight at 4°C and purified by precipitation in cold ethanol and subsequently re-dissolved in water. The mixture was then dialyzed for two days, using a dialysis membrane with a molecular weight cut-off (MWCO) of 10-14 kDa against water at 4°C. The polymer solution was freeze-dried, and the recovered polymer was then referred to as HAMA.

Synthesis of glycidyl methacrylated hyaluronic acid (HAGM)

HAGM was synthetized using a previously described protocol[19]. Briefly, 10% (w/v) of HA sodium salt (1.6 MDa, Sigma Aldrich) was dissolved in 200 mL of deionized water for 12 h under vigorous stirring. Once dissolved, 8.0 mL of

triethylamine (Sigma Aldrich), 8.0 mL glycidyl methacrylate (Sigma Aldrich), and 4.0 g of tetrabutyl ammonium bromide (TBAB) (Sigma Aldrich) were added separately. Each component was allowed to fully mix for 1 h before the next addition. Following complete dissolution, the flask was opened slightly and incubated at 55°C for 1 h. After cooling, the solution was precipitated in 20 times excess volume of acetone (4 L), resulting in the formation of solid white fibers. The precipitate was then dissolved in ultrapure water, dialyzed, and freeze-dried.

Proton nuclear magnetic resonance (^{1}H NMR) characterization of synthesized polymers

All polymers were dissolved separately in dimethyl sulfoxide-d6 (6 mg/mL) and incubated at 50°C overnight. ^{1}HNMR spectra was then recorded by applying a 10 s recycle delay for 64 scans at ambient temperature using a Bruker DRX400 spectrometer operating at 400 MHz. The degree of methacrylation (DM) of the HAGM was determined by digital integration of the anomeric proton signals or methyl protons signals (H) of HA at 2.0 ppm and of the methacrylate (MA) proton signals (H') at ~6.1, ~ 5.7, or ~1.93 ppm. The DM of HAMA was determined by digital integration of the anomeric proton signals or methyl protons signals (H) of HA at 2.6 ppm, and of the MA proton signals (H') at ~6.3, ~6.7, or ~2.5 ppm, as described previously by Hachet E *et al*.[18] using **Eq. 1**.

$$DM\,(\%) = \frac{(I_{H'}\,(methyl\ proton\ on\ MA)\ /\ 3)}{(I_H\,(methyl\ proton\ on\ HA)\ /\ 3)} \times 100 \quad (\mathbf{Eq.\,1})$$

The DM of gelatin molecules (B300 or B225) in GelMA was defined as the percentage of amino groups of gelatin (lysine and hydroxylysine) that were modified in GelMA. The two protons of the methacrylate double bond gave rise to two signals at 5.3 and 5.6 ppm. The lysine methylene signals (2.8–2.95 ppm) of the non-modified gelatin spectra and GelMA spectra were integrated separately to obtain the areas of lysine methylene, according to a previously defined method by Hoch E. *et al*[20]. The DM of GelMA was calculated by using **Eq. 2**.

$$DM\,(\%) = 1 - \frac{(lysine\ methylene\ of\ GelMA)}{(lysine\ methylene\ of\ gelatin)} \times 100 \;(\mathbf{Eq.\,2})$$

The DM of PEGDA was defined as the percentage of two distal hydroxyl groups of PEG molecules that were modified with acrylate groups. The chemical shift located at 5.9–6.4 ppm was assigned to the protons of vinyl groups. By comparing the integration ratio between one of the proton signals (H') of the vinyl units (e.g., at ~6.2 ppm) and the signal (H) of the terminal methylene of PEG (~ 4.1 ppm), the degree of acrylation (DA) of PEG was calculated according to a previously defined method by Tan F. *et al*[17] using **Eq. 3**.

$$DA\,(\%) = \frac{(I_{H'}(vinyl\ proton\ of\ acrylate))}{(I_H(methylene\ of\ PEG))} \times 100 \quad (\mathbf{Eq.\,3})$$

GelPatch hydrogel formation

A visible light-sensitive photoinitiator (PI) system was used to crosslink the pre-polymers into solid adhesive hydrogels. The PI solution was prepared by dissolving 0.5 mM Eosin Y (photoinitiator; Sigma Aldrich), 1.87% (w/v) triethanolamine (co-initiator), and 1.25% (w/v) N-Vinylcaprolactam (co-monomer) in DPBS. Hydrochloric acid was used to adjust the pH of the final solution to 7.4. Different hydrogel formulations were prepared by dissolving various concentrations of different polymers in the PI solution. The GelMA (B300 and B225) polymers were tested at different concentrations of 3.0, 4.0, 6.5, and 7.0% (w/v), PEGDA at 0.5 and 1.0% (w/v), HAMA at 0.5, 1.0, and 3.0% (w/v), and HAGM at 0.5 and 3.0% (w/v) (**Table S1**). After complete dissolution, the hydrogel solutions were crosslinked for 4 min by exposure to visible light (450 to 550 nm) using a LS1000 Focal Seal Xenon Light Source (100 mW/cm^2, Genzyme).

Mechanical characterization

For mechanical tests, 75 µl of hydrogel precursor solution was pipetted into polydimethylsiloxane (PDMS) cylindrical molds (diameter: 6 mm; height: 2.5 mm). The resulting solution was photocrosslinked by visible light for 4 min. After photocrosslinking, the dimensions of the hydrogels were measured using a digital caliper. Compression tests were conducted using an Instron 5542 mechanical tester. The crosslinked hydrogel cylinders were compressed at a rate of 1 mm/min until failure was achieved. The slope of the stress-strain curves was obtained and reported as the compression modulus.

Measurement of weight swelling ratio

Hydrogel samples were prepared as described previously. The weight of each hydrogel sample was measured following photocrosslinking and after 24 h of incubation in DPBS at 37°C. The swelling ratio was then calculated according to **Eq. 4**, where W_0 is the weight of the sample immediately after photocrosslinking and W_1 is the final weight of the sample after 24 h of incubation.

$$Swelling\ ratio\,(\%) = \frac{W_1 - W_0}{W_0} \times 100 \quad (\mathbf{Eq.\,4})$$

In vitro burst pressure

Burst pressure resistance of the hydrogel formulations was measured using the modified American Society for Testing and Materials (ASTM) F2392-04 standard according to a previously reported method[14]. Briefly, collagen sheets from porcine intestines (4 × 4 cm) were placed between two stainless steel annuli from a custom-built burst pressure device, consisting of a metallic base holder, a pressure sensor, a syringe pressure setup, and a data collector. A hole

(2-mm diameter) was created through the sheet and was sealed by photocrosslinking 30 µl of hydrogel precursor solution. Next, airflow was applied into the system, and the burst pressure was recorded until detachment of the hydrogel from the collagen sheet and/or rupturing. The burst pressure resistance was measured using a pressure sensor (PS-3203, PASCO Scientific, Roseville, CA).

Enzymatic degradation

In vitro degradation of GelPatch formulations was determined as described previously[16]. Cylindrical (diameter: 6 mm; height: 2.5 mm) hydrogels were formed as described previously. Samples were incubated in DPBS supplemented with various concentrations (0.5 to 20 µg/mL) of collagenase type II and hyaluronidase (degradation media) at a ratio of 1:1 for 5 days. At each time point (0, 1, 3, and 5 days), samples were removed, freeze-dried, and weighed. The media was refreshed at each time point. The degradation percentage of each sample was calculated based on the weight loss at different time points (W_h) as compared to the initial weight (freeze dried samples) at time 0 (W_0) following **Eq. 5**.

$$\text{Degradation (\%)} = \frac{W_0 - W_h}{W_0} \times 100 \qquad (\textbf{Eq. 5})$$

Rheological measurement

Oscillatory rheology measurements of hydrogel precursor solutions were carried out with an Anton Paar (MCR 302) by utilizing a cone plate (radius 8-mm, cone angle 2°). A solvent trap was used to minimize water evaporation during the measurement. All rheology measurements were performed at 25°C. Amplitude sweeps, with shear rates (γ) ranging from 0.1 to 100 per second at 25°C under flow conditions, were performed at a frequency of ω= 1 Hz/s.

Degree of porosity

The volume fraction of voids (V_v) was used to define the degree of porosity of hydrogel patches through measuring the bulk density (ρ) of the hydrogel. The apparent density (ρ*) of the hydrogel cylinder was calculated by measuring the volume and weight. The porosity was then calculated using **Eq. 6**[21, 22].

$$Vv = 1 - \frac{\rho *}{\rho} \times 100 \qquad (\textbf{Eq. 6})$$

Brightfield microscopy

An aliquot of 30 µL of freshly prepared hydrogel precursor solution was pipetted on glass slides and covered with a coverslip prior to microscopy. Brightfield microscopy photos were taken using a ZEISS Axio Observer Z1 inverted microscope at 10X objective.

Computerized Definitive Screening Design (DSD)

A Design of Experiment (DoE) method was applied to better understand the relationship and the correlation between the response variables and experimental factors[23]. In this study definitive screening design (DSD)[24] was applied which allowed us to study the effects of a large number of factors with a relatively small set of experiments. This design was able to estimate main and quadratic effects in addition to the secondary effects between the factors[25]. Each factor had multiple levels to determine non-linear correlations. The experimental data were analysed with JMP® 16 software (SAS Institute). Multiple regression analysis was performed to identify the critical factors per response parameter. This multiple regression analysis was approximated by a step wise selection technique. Significance was considered for p values with $p \leq 0.05$ (accounting for main effects and interactions). Data was collected from a five-factor design, each with various levels, allowing us to study the effects of the experimental factors on the response parameters. The summary of the design is shown in **Table S1**.

In vitro biocompatibility

In vitro tests were performed to assess biocompatibility of the hydrogel patches using two techniques: 1) direct seeding (2D culture) and 2) indirect seeding (elution test) using human telomerase immortalized corneal epithelial cells (hTCEpi) (provided by Dr. Argueso, Schepens Eye Research Institute, Mass Eye and Ear, Boston MA) and human corneal endothelial cells (HCEC), respectively.

For direct seeding, the cells were seeded on the surface of hydrogel scaffolds as described previously[26, 27]. Briefly, 10 µL of GelPatch precursor solutions were spread and photocrosslinked on a 3-(Trimethoxysilyl) propyl methacrylate (TMSPMA)-coated glass slide, providing a 1 x 1 cm² surface area of hydrogel. Samples were placed in a 24 well-plate and hTCEpi cells were seeded on the hydrogel surface (10^5 cells per sample). After incubation of the seeded samples in a humid incubator with 5% CO_2 for 1 h at 37°C, 400 µL of media was added to each well and incubated for 24 h. The media was replaced with fresh media every other day. The viability of cells cultured on the selected GelPatch formulation (G7HG3) was evaluated at day 1 and 3 using a Live/Dead™ Viability/Cytotoxicity Kit (Invitrogen) according to the manufacturer's instructions. Briefly, a solution of calcein AM at 0.5 µL/mL (green color, viable cells) and ethidium homodimer at 2 µL/mL (red color, non-viable cells) in DPBS was used to stain cells. After 15 min of incubation, samples were washed with DPBS, and cells were imaged using a fluorescence optical microscope (Primovert, Zeiss). The collected images were analysed using ImageJ software to quantify cell viability (%) by dividing the number of live cells by the total number of live and dead cells. The proliferation and metabolic activity of cells were determined using PrestoBlue assay (Invitrogen) at day 1 and 3 post-seeding according to the manufacturer's instructions. Briefly, a media solution containing 10% PrestoBlue reagent was added to the seeded samples and incubated for 45 min

at 5% CO_2 at 37°C. The fluorescence intensity of the solution was determined using a plate reader (BioTek) at 540 nm (excitation)/600 nm (emission).

The morphology of the cells and their expansion were assessed through staining of F-actin filaments with Alexa Fluor 594–phalloidin (Invitrogen) to visualize the cytoskeleton, and cell nuclei were visualized with DAPI. In short, cells were fixed with 4% (w/v) paraformaldehyde for 15 min, permeabilized using 0.3% (v/v) Triton in DPBS for 10 min and blocked with 1% (w/v) bovine serum albumin (BSA) in DPBS for 30 min at room temperature. Samples were serially incubated with phalloidin (1:400 dilution in 0.1% BSA) and DAPI (1:1000 dilution) solution for 45 min and 1 min, respectively. The samples were washed and imaged using a Zeiss fluorescent microscope.

The elution test method was conducted according to ISO10993-1 standard. Cells were cultivated in 48-well plates. Extracts were obtained by incubating photocrosslinked hydrogels with varying polymer ratios in 1 mL of Keratinocyte Cell Basal Medium (KBM Gold Basal Medium, 00192151, Lonza) supplemented with KGM Gold SingleQuots (001921152, Lonza) at 37°C for 24 h. After 3 days of incubation at 37°C, fluid extracts were then applied to a confluent HCEC monolayer. Control groups were prepared similarly by incubating the cells with fresh media. After 1 day of incubation at 37°C, cells were stained with calcein-AM and Ethidium homodimer as described before and imaged with an inverted fluorescence microscope. *In vitro* PrestoBlue was also performed on each group following manufacturer protocols (n = 9 per formulation).

Ex vivo burst pressure test

For burst pressure tests, fresh New Zealand white rabbit eyes (harvested within 24 h) were purchased from Sierra for Medical Science and hydrogel formulations were tested on 2-mm incisions on (i) the cornea and (ii) the sclera. A 2-mm linear full thickness incision was created on the cornea using a surgical 22.5° ophthalmic knife (Alcon). Similarly, to create scleral lacerations, the conjunctiva of rabbit eyeballs was removed and a 2-mm linear full thickness incision was created. Hydrogel formulations were applied on the incision site utilizing a contact lens (methafilcon A, 55% water, diameter 15, base curve 8.30, Kontur Kontact, Hercules, CA) trephined to a 6-mm diameter (sclera: n=9, cornea: n=4). The hydrogel was then crosslinked for 4 min by visible light. ReSure® sealant was used as a control for burst pressure studies (sclera: n=4; cornea n=4). Intra-ocular pressure (IOP) was then increased by injecting DPBS via an infusion cannula until detachment of the hydrogel or leaking at the incision site. The pressure was recorded by an attached sensor (PS-3203, PASCO Scientific, Roseville, CA).

Ex vivo assessment of GelPatch retention to the sclera and subconjunctival space

For retention studies, fresh New Zealand white rabbit eyes (harvested within 24 h) were purchased from Sierra for Medical Science. Excess muscle was removed from eyes while keeping the bulbar conjunctiva intact and placed in a 2.5% povidone-iodine solution (Betadine; Purdie Products, Stamford, CT) for 1 min and rinsed twice with DPBS. Two methods were utilized to test GelPatch adhesion to the sclera: 1) subconjunctival injection and 2) direct scleral application. Subconjunctival injection allowed for the application of the GelPatch to the sclera without the need to remove overlying conjunctival tissue. For this test, the optimized GelPatch formulations composed of 7% (w/v) GelMA(B300) and 3% (w/v) HAGM (G7HG3), and 14% (w/v) GelMA(B300) and 3% (w/v) HAGM (G14HG3), were loaded into a syringe with an 18 G needle. The needle tip was inserted into the subconjunctival area and a 4 mm x 4 mm pocket was created before depositing 20 µl of bioadhesive into the subconjunctival space. For direct scleral application of the bioadhesive, the site of application was prepared by removing overlying conjunctival tissue to reveal the underlying sclera. After drying of the area, 20 µl of bioadhesive was applied to a contact lens applicator and placed directly on the sclera to be crosslinked by visible light for 4 min. Then, the rabbit eyes were placed into 6 well plates and 2%-agar (Sigma) Dulbecco's Modified Eagle's medium (DMEM; Sigma) supplemented with 10% Fatal Bovine Serum (FBS; Atlanta Biologicals, Flowery Branch, GA) secured the eyes in wells. DMEM supplemented with 10% FBS and 1% penicillin- streptomycin solution was added to a height of 50% eye depth and incubated in a humidified 5%-CO_2 incubator at 37°C and media was replaced every day. The adhesion of the bioadhesives to the sclera was assessed daily for up to 4 days. For the subconjunctival application group, the overlying conjunctiva was first removed 24 h after initial bioadhesive application using forceps and surgical scissors. Adhesion was tested manually using an eye spear tip (DeRoyal Industries, Powell, TN) hydrated with DPBS, and passed over the bioadhesive three times to assess retention and adhesion.

Statistical analysis

All experiments were tested at least 3 times, and generated data were expressed as mean ± standard deviation. Data analysis was conducted using either t-test, one-way or two-way ANOVA, followed by Tukey's test or Bonferroni test (*$p < 0.05$**$p < 0.01$, ***$p < 0.001$ and ****$p < 0.0001$) using GraphPad Prism 6.0.

Results and Discussion

Physicochemical characterization of single components

In this study, we used a systematic approach to design and optimize a photocrosslinkable adhesive hydrogel, GelPatch, for sealing of sclera or subconjunctival tissues (**Fig. 1**). For this study, three main functionalized polymers (GelMA, HAMA or HAGM, and PEGDA) were utilized. GelMA was used to form the main matrix and was the main tissue adhesive component of the GelPatch due to its high number of functional groups and high degree of methacrylation. HAMA or HAGM polymers, with high molecular weights, were
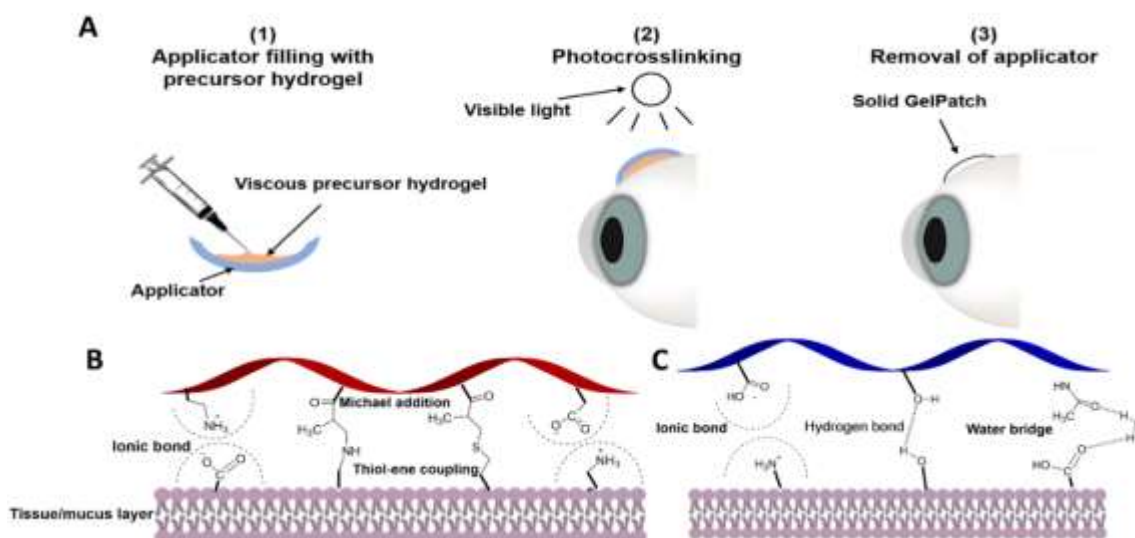
Figure. 1. Molecular structure, application, and adhesion mechanism of GelPatch). (A) Schematic of GelPatch application. (1) Applicator (e.g., a contact lens) filled with precursor hydrogel. (2) Then, the applicator containing the hydrogel precursor is directly applied onto the scleral surface and photocrosslinked by visible light to form a solidified soft hydrogel. (3) After photocrosslinking, the applicator can be removed, leaving behind only the adhesive hydrogel. Schematic representation of the possible chemical and physical bond formations at the hydrogel/eye tissue interface with the (B) GelMA polymer chain and (C) HAGM polymer chain with the existing functional groups of the target ocular tissue.

added at lower concentrations to improve the viscoelastic properties of the GelPatch prepolymer solutions in the liquid state. In addition, HAGM, with high molecular weight and specific degree of glycidyl methacrylate (~12%) to increase elasticity of the crosslinked GelPatch formulation without enhancing the stiffness. PEGDA, at the fixed molecular weight of 35 kDa, was also included in the hydrogel formulation to assess its impact on overall characteristics of the hydrogel such as mechanical properties, swelling ratio, and adhesion to the biologic surface.

To formulate the GelPatch, HA, gelatin, and PEG were first chemically modified to form photocrosslinkable polymers. The modified polymers were characterized for the degree of substitution of methacrylate groups using ^{1}HNMR analysis **(Table S2)**. The degree of methacrylation for GelMAs (B300 and B225) were calculated to be 81% and 78%, respectively (**Figs. S1 and S2**). The degree of glycidyl methacrylation of HAGM and methacrylation of HAMA was calculated to be 12% and 33%, respectively (**Figs. S3 and S4**). Finally, the degree of acrylation for PEGDA was calculated to be 85% **(Fig. S5)**.

For single component characterization of the hydrogel prepolymers, the precursor solution of individual polymers was prepared at a total polymer concentration of 10% (w/v) for both types of GelMA-based hydrogels (B300 and B225) and at the concentration of 3% (w/v) for HAMA and HAGM, respectively. The precursor solution of PEGDA was prepared at 1% (w/v), which was the maximum PEGDA concentration used in this study. Precursor solution of PEGDA was not crosslinkable at the concentration of 1% (w/v), therefore the single component characterization of crosslinked PEGDA was not feasible. The rheological properties of the individual polymer precursor solutions (i.e., liquid state) were studied. Viscosity of different polymer solutions, measured at a

shear rate of 0.1 (1/s), showed the highest viscosity of 557.3 ± 10.4 Pa. s for 3% (w/v) HAMA precursor solution. Comparatively, for HAGM, at the same concentration, viscosity was lower at 60.4 ± 4.5 Pa. s **(Fig. 2A-B).** At the shear rate of 0.1 (1/s), viscosities of 10% (w/v) GelMA B300 and GelMA B225 precursor solutions were 0.13 ± 0.06 Pa. s and 0.07 ± 0.03 Pa. s, respectively. The measured viscosity for 1% (w/v) PEGDA was 0.001± 0.0006 Pa. s. The viscosities of GelMA B300, GelMA 225, and PEGDA were not affected by the shear rate, indicating the Newtonian behaviour of these precursor solutions. One of the critical parameters in the development of an ocular sealant or patch is the initial viscosity at the point of application and the yield stress. In general, a high initial viscosity is required for retention of the hydrogel prepolymer solution upon application and before crosslinking at the site of injury. Intact ocular tissue is moist, and some ocular injuries can be highly perfusive, which can cause dilution of the applied precursor solution, thereby decreasing the crosslinking efficiency. Therefore, HAMA and/or HAGM are essential components in the formulation of our ocular hydrogel patch. The representative viscosity curves as a function of shear rate for HAMA and HAGM hydrogels are shown in **Fig. 2B**. The obtained results showed that differences in the degree of methacrylate substitution of HA, as well as the type of substitution based on either hydroxyl reacted methacrylate anhydride or carboxyl reacted glycidyl methacrylate, significantly impacted the viscosity of the hydrogel precursor solution. As shown in **Fig. 2B**, HAMA showed a significantly higher viscosity as compared to HAGM.

In general, adhesion of photocrosslinked methacrylated polymers to biologic surfaces is mainly due to the electrostatic interaction and/or chemical bonds at the tissue-polymer interface[28]. The existing functional groups in the polymer chains such as hydroxyl, carboxyl, and amine can interact with the functional groups at the
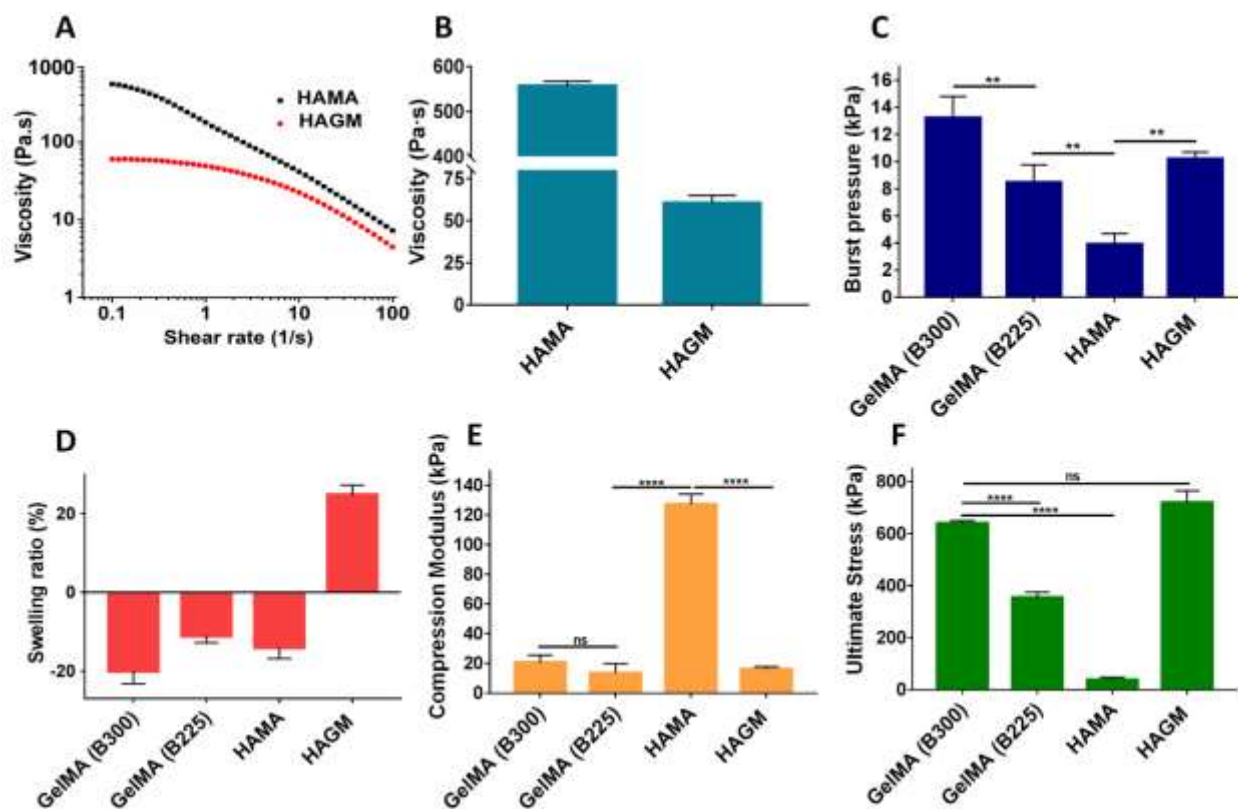
Figure 2. Characterization of prepolymer solution and crosslinked hydrogels formed based on single polymers. (A) Viscosity of HAGM and HAMA as a function of shear rate at 25°C. (B) Viscosity of single polymer-based precursor solutions determined at a shear rate of 0.1 (1/s). (C) Burst pressure of photocrosslinked hydrogels formed based on single polymers. (D) Swelling ratio (%) of photocrosslinked hydrogels formed based on single polymers within the first 24 h upon incubation in DPBS at 37°C. (E) Compression modulus and (F) ultimate strength of photocrosslinked polymers. Data are represented as mean ± SD (*p<0.05, **p<0.01, ***p<0.001, ****p<0.0001)

tissue surface[28]. Essentially, the methacrylated groups along the polymer chains can interact with the tissue via Thiol-Ene reaction and/or Michael addition upon exposure to visible light[29] **(Fig. 1B-C).** Other parameters that may impact the adhesion of crosslinked polymers include, but are not limited to, 1) the degree of entanglement and interpenetration of the polymer chains at the tissue hydrogel interface, 2) the swelling ratio of crosslinked polymers, and 3) the shape fidelity of the crosslinked hydrogels at the tissue surface (specifically for surfaces with curvatures)[30]. The conformation of protein chains in the precursor hydrogel solution may also impact the tissue adhesion due to two main effects: 1) increased accessibility of functional groups which will allow for increased chemical or ionic bond formation at the tissue/hydrogel interface and 2) the interpenetration and entanglement of polymer chains across the contacting surface of the target tissue which will enhance the adhesive properties of the hydrogel patch to the tissue[31].

Before*, in vitro* adhesion test, the circular dichroism (CD) spectra of GelMA B300 and GelMA B225 were used to investigate the conformational changes in GelMA chains compared to unmodified gelatin. The CD spectra of gelatin showed a sinusoidal CD spectrum consisting of a positive band at 220 nm, and a

negative band with a peak at approximately 198 nm, which were characteristic of the triple-helical structure (**Fig. S6**). However, a decrease in the CD spectra at 198 nm, for GelMA B300 and GelMA B225, could be the typical characteristic of the random coil conformation of methacryloyl modified polypeptide chains of gelatin. This change in conformation can be due to the breaking of inter- and intramolecular ionic bonds as well as hydrogen bonds and other Van der Waals interactions within the GelMA polymer solution, thereby changing its native conformation[32, 33]. We hypothesize that the random coil conformation of polymer chains in the precursor hydrogel solution is the most preferred conformation. This conformation may maximize chemical and physical interactions of the functional groups in the polymer with the tissue due to an increase in their accessibility and the excess freedom in their backbone motions compared to the triple helix conformation[34, 35].

To this end, the adhesive properties of the single polymer-based hydrogels were measured based on a standard burst pressure test. Our results showed that GelMA B300 had the highest burst pressure of 13.2 ± 1.6 kPa. Among all the formulations, HAMA showed the lowest burst pressure value of 3.9 ± 0.8 kPa. GelMA B225 and HAGM showed burst pressures of 8.5 ± 1.3 kPa and 10.2

± 0.5 kPa, respectively **(Fig. 2C)**. The results also showed that among the two types of GelMA-based hydrogels with different molecular weight distributions, the GelMA hydrogel with a higher molecular weight, GelMA B300, had a higher burst pressure compared to GelMA with a lower molecular weight, GelMA B225. The lower burst pressure value of HAMA compared to HAGM can be attributed to the high degree of stiffness of HAMA compared to HAGM upon crosslinking and the lack of flexibility, therefore, this relationship can be attributed to the lack of shape accommodation that is due to gradual increase in curvature formation on the collagen sheet upon applying air pressure during testing.

The results of water uptake capability of the single polymer-based hydrogels showed that swelling values obtained for GelMA formulations (B300 and B225) were -20 ± 3.2 % and -11 ± 1.8 %, respectively, after 24 h. The negative values in the swelling ratio

contribute to repulsion of water molecules. The results for crosslinked HA-based hydrogels showed shrinking for the HAMA hydrogel (-13.9 ± 2.8 %) and swelling for the HAGM hydrogel (24.7 ± 2.6 %) **(Fig. 2D)**. In general, HAGM had a lower degree of methacrylation as compared to HAMA, which caused a decrease in crosslinking density and consequently an increase in the swelling ratio. Another factor contributing to this relationship was the difference in the molecular structure of glycidyl methacrylate (the majority of the methacryloyl substitutes of HAGM) compared to the methacrylated groups of HAMA. The glycidyl methacrylate group can form hydrogen bonds which may result in an increase in the swelling ratio of HAGM hydrogel.

The results of mechanical characterization of single polymer-based hydrogels showed that among all hydrogels, HAMA had the highest modulus of 127.0 ± 7.1 kPa with an ultimate stress of 38.0 ± 10.4 kPa, therefore, indicating high rigidity of the crosslinked
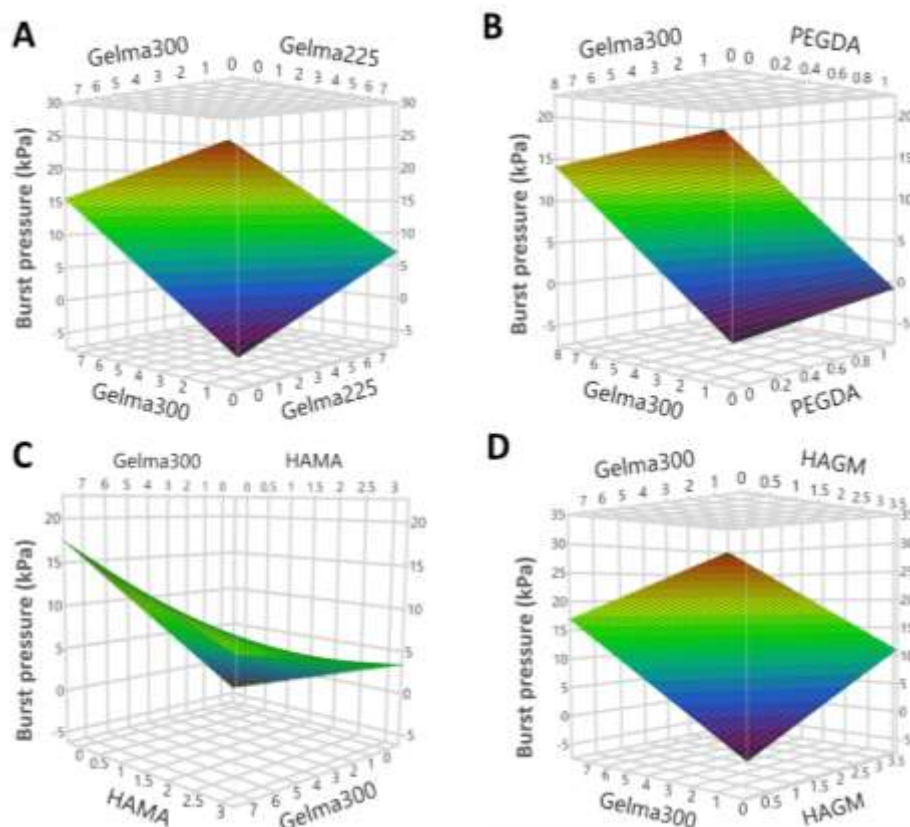

Figure 3. Response surface estimated by definitive screening design (DSD) for the burst pressure (A) as function of GelMA B300 and GelMA B225 concentrations, (B) as function of GelMA B300 and PEGDA concentrations, (C) as function of HAMA and GelMA B300 concentrations, (D) as function of GelMA B300 of HAGM concentrations. Only positive Z values were considered.

of the hydrogels indicate shrinking of the hydrogels upon incubation at 37°C in DPBS. This might be due to the existing hydrophobic (proline rich) domains along the porcine GelMA polymer chains, which form hydrophobic interactions at 37°C and consequently repel water molecules. Other factors that contribute to the shrinking properties of the hydrogels could be the high degree of crosslinking for both GelMA-based polymers due to the high degree of methacrylation, which could also

HAMA Hydrogel. The compression modulus for HAGM was 16.1 ± 1.7 kPa with an ultimate stress of 719.8 ± 46.3 kPa. GelMA B300 and GelMA B225 showed moduli of 20.52 ± 5.1 kPa and 13.4 ± 6.3 kPa with ultimate stress of 640.2 ± 10.3 kPa and 335.6 ± 20.5 kPa, respectively (**Figs. 2E-F, S7**). In general, the obtained results show that 3% (w/v) HAMA is less resistant to deformation and is less elastic. The modulus of the developed material may impact the overall performance of the patch for ocular applications. For

instance, highly rigid adhesives can cause a foreign body sensation and irritation upon blinking (i.e., applied shear stress). The development of a non-rigid (soft) ocular patch (modulus of ≤ 30 kPa) with elastic properties (strain of ≥ 50%) is highly preferable for eye application.

Modeling and screening of hydrogel formulations based on pre-defined selection criteria

With the information obtained from the previous section on physicochemical characteristics of single polymers, we next prepared GelPatch formulations based on different combinations and concentration of polymers provided by DSD (**Table S1**). Our primary goal was to investigate the effect of five factors on predefined response parameters for the optimized GelPatch formulation (**Table 1**). These response parameters included burst pressure, swelling ratio, mechanical strength, and elasticity of GelPatch formulations. The five variables applied in this study were: 1) two different molecular weights of GelMA polymer (B300 and B225), 2) two different degrees of methacryloyl substitution on HA molecules (HAMA and HAGM), and lastly 3) the addition of PEGDA in the formulations. After characterization of different formulations, we applied DSD to fit a model for the

obtained data and statistically verify the most significant factors impacting GelPatch properties (i.e., response parameters). We also evaluated the correlation between different factors and response parameters, and screened for the most optimized formulation to be applied for the *in vitro* and *ex vivo* functional testing. The coefficient of determination for all response parameters was ≥0.9 (**Fig. S8**). This indicates that the applied model can predict ≥90% of variations in the response parameters via changing the variables. The mode of contribution of these factors to response parameters was then assessed using the t-ratios and p-values. Our design showed that, GelMA B300 and HAGM significantly enhanced the burst pressure (p <0.0001). In contrast, the addition of HAMA (p = 0.92) or the combination of HAMA with GelMA B300 (p = 0.56) and HAMA with PEGDA (p = 0.68) decreased the burst pressure of the resulting hydrogel **(Table 2)**. Furthermore, PEGDA had no impact on burst pressure (p = 0.94). GelPatch formulations with higher burst pressures were obtained with compositions containing GelMA B300 and HAGM, and reduced concentrations of HAMA **(Fig. 3)**. For the swelling ratio, the presence of both PEGDA and HAGM in the GelPatch formulations significantly enhanced the swelling ratio (p<0.0001). In addition, based on

Table 1. Selection criteria for the identification of the optimized GelPatch formulation with desired properties.

	Property	Desirable range of values	Rationale
	Total polymer concentration	≤10 wt%	Handling, biocompatibility, and less ocular sensation
Solid state	Burst pressure	≥15 kPa	Retention on the ocular tissue surface
	Swelling	≤20%	To prevent shape deformation and provide a lubrication effect at the polymer tissue interface
	Modulus	≤30 kPa	Shape accommodation, curvature formation, minimize ocular sensation
	Elasticity	≥50%	Shape accommodation and curvature formation
Liquid state	Viscosity at low shear	≥10 Pa.s, ≤60 Pa.s	No run off, shape fidelity, and injectability
	Yield stress	≥100 Pa	Handling and no flow upon application

Table 2. Ranking of the contribution of different factors and their interactions on burst pressure and swelling ratio, analyzed by DoE. The red colored values indicate statistically highly significant (p <0.0001) and the blue-colored values indicate moderately significant (p >0.0001 and p <0.05).

Rank	Burst pressure			Swelling ratio		
	Factor	t-ratio	p-Value	Factor	t-ratio	p-Value
1	GelMA (B300)	5.07	<0.0001	GelMA (B300)	0.56	0.58
2	GelMA (B225)	3.41	0.002	GelMA (B225)	1.27	0.21
3	PEGDA	0.07	0.94	PEGDA	5.85	<0.0001
4	HAGM	10.07	<0.0001	HAGM	18.68	<0.0001
5	HAMA	0.11	0.92	HAMA	-2.46	0.021
6	GelMA(B300) *HAMA	-0.58	0.56	GelMA(B225)*PEGDA	2.95	0.0071
7	PEGDA*HAMA	-0.41	0.68			

t-ratios, GelMA B225 had a higher impact on swelling (t-ratio= 1.27) as compared to GelMA B300 (t-ratio = 0.56). In general, the addition of HAMA to the formulation decreased the swelling ratio (p = 0.021) and even caused shrinking of the GelPatch at a concentration of 3% (w/v). This characteristic of HAMA can be attributed to its molecular structure and the presence of carboxylic groups, which can cause complex coacervation and water expulsion when mixed with GelMA or other polymers that contain a high density of cationic moieties[36]. In contrast, the combination of GelMA B225 and HAGM increased the swelling ratio significantly (p = 0.007) which is incompatible with our desired characteristics **(Table 2)**.

For compression modulus, HAMA and GelMA B300 significantly enhanced the strength (modulus) of the crosslinked hydrogels (p<0.0001 and p<0.0005, respectively). A combination of HAMA with GelMA B300 significantly increased the modulus (p<0.0001) **(Table 3)**. However, the combination of HAGM with GelMA B300 showed moderate increase in modulus (p = 0.023) as compared to the previous formulation. Regarding the elasticity of the crosslinked hydrogels, HAGM significantly enhanced the elasticity (p = 0.0008). Conversely, HAMA had the opposite effect and significantly decreased the elasticity (p<0.0001). The addition of PEGDA to the formulation had less impact on elasticity (p = 0.051) compared to HAGM. No significant impact on elasticity was detected from GelMA B300 and GelMA B225. The overall results suggest that among all the components, HAGM and GelMA B300 had the highest positive impact on adhesion. HAMA negatively impacted the swelling ratio. Compression modulus of GelPatch could be improved significantly via addition of GelMA B300, HAMA, or a combination of both. Finally, among all the components, HAGM could improve elasticity, and HAMA negatively impacted the elastic properties of the GelPatch. A graphical overview of the predicated model for each response parameter was depicted in the form of response surface (3D charts). The response surface of two factor interactions for the burst pressure is reported in **Fig. 3**. The results showed that the mode of

contribution of all factors on burst pressure was linear **(Fig. 3 A-B & D)** except for HAMA, which showed a non-linear correlation in the presence of GelMA B300 **(Fig. 3C)**. The results also showed a positive correlation between GelMA B300 and HAGM, and GelMA B300 and GelMA B225. Increasing PEGDA concentrations in the presence of GelMA B300 had no significant effect on burst pressure. These results were in agreement with the reported t-ratios and p-values in **Table 2**.

The response surface for the swelling ratios (%) showed significant decrease in swelling with an increase in concentration of GelMA B300 in the presence of GelMA B225 **(Fig. S9)**. The two-factor interactions between GelMA B300 and PEGDA showed a linear increase in swelling ratio with an increase in PEGDA concentration. The presence of GelMA B300 in the formulation had less effect on swelling ratio (%). Both GelMA B300 and HAMA showed linear correlations and decreased the swelling ratio with an increase in their concentrations. The two factor interactions between HAGM and GelMA B300 showed the opposite effect. A sharp increase in swelling ratio with an increase in HAGM concentration and decreased swelling ratio with increased GelMA B300 concentration were observed **(Fig. S9)**. Regarding the compression modulus, no impact was observed for GelMA B225 when combined with different concentrations of GelMA B300 **(Fig. S10)**. Combination of PEGDA with GelMA B300 did not cause any significant change in the compression modulus. The two factor interactions between GelMA B300 and HAGM showed a moderate increase in response by increases in their concentrations. However, a nonlinear response at different concentrations of GelMA B300 and HAMA was detected. HAMA showed a higher impact on increasing the modulus as compared to GelMA B300 **(Fig. S10)**. These results were in agreement with the reported t-ratios and p-values in **Table 2**.

The response surface plots on elasticity showed a decrease in response with increased concentrations of both GelMA B300 and GelMA B225 **(Fig. S11)**.

Table 3. Ranking of the contribution of different factors and their interactions on compression modulus and elasticity, analyzed by DoE. The red-colored values indicate statistically highly significant (p <0.0001) and the blue-colored values indicate moderately significant (p >0.0001 and p <0.05).

Rank	Compression Modulus			Elasticity		
	Factor	**t-ratio**	**p-Value**	**Factor**	**t-ratio**	**p-Value**
1	GelMA (B300)	4.04	<0.0005	GelMA(B300)	-1.21	0.24
2	GelMA (B225)	-1.52	0.14	GelMA (B225)	-0.58	0.57
3	PEGDA	0.21	0.83	PEGDA	2.04	0.051
4	HAGM	2.26	0.034	HAGM	3.78	0.0008
5	HAMA	17.59	<0.0001	HAMA	-5.96	<0.0001
6	GelMA(B300) *HAMA	5.55	<0.0001			
7	GelMA(B300) *HAGM	2.43	0.023			

Biomaterials Science

ARTICLE

An increase in PEGDA concentration had less impact on the elasticity of the resulting hydrogel. The two factor interactions between GelMA B300 and HAMA showed a decrease in elasticity with an increase in concentrations of both polymers. HAMA showed a higher impact on decreasing the elasticity of the formed GelPatch as compared to GelMA B300. A combination of GelMA B300 and HAGM showed the opposite response on elasticity. A sharp increase in elasticity with an increase in HAGM concentration and decreased elasticity with an increase in GelMA B300 concentration was observed **(Fig. S11)**.

Characterization of the most desirable hydrogel patch formulations

Among all hydrogel combinations, JMP software selected the most desirable combinations based on the applied model and predefined selection criteria. The selected combinations were characterized for burst pressure and swelling ratio which are two of the most important response parameters for GelPatch. Among all the formulations, the formulation containing 7% (w/v) GelMA B300 and 3% (w/v) HAGM (abbreviated as G7HG3), showed the highest burst pressure value of 26.5 ± 2.8 kPa. The lowest value obtained for burst pressure was 5.6 ± 1.2 kPa for the formulation composed of 1% (w/v) PEGDA and 3% (w/v) HAMA (P1HA3). The formulation composed of 7% (w/v) GelMA B225 and 3% (w/v) HAMA (abbreviated as
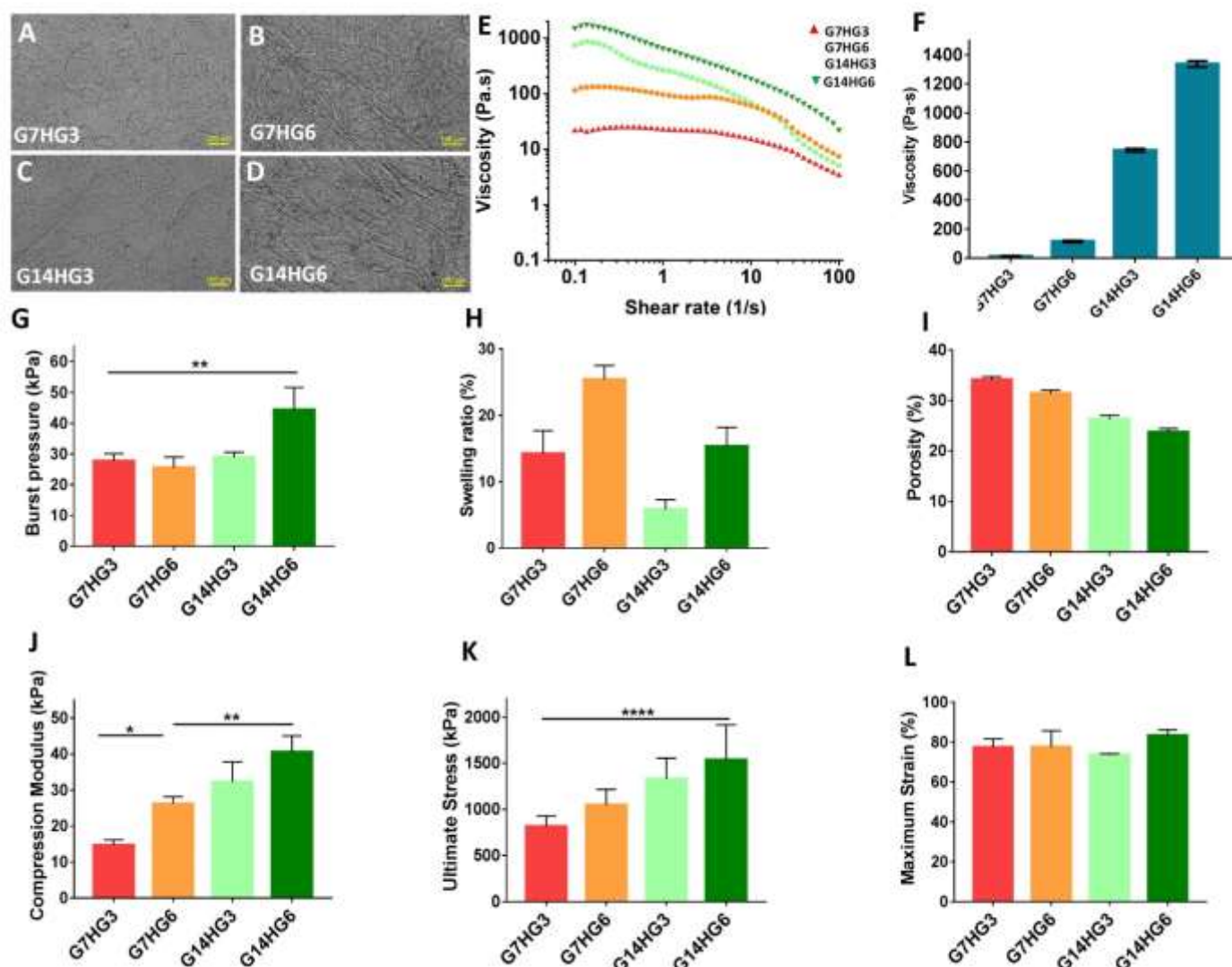

Figure 4. Physical Characterization of GelPatch formulations in liquid and solid states. Liquid state: Bright field microscopy images of (A) G7HG3, (B) G7HG6, (C) G14HG3, and (D) G14HG6 hydrogel precursor solutions at 25°C, (E) Viscosities of different hydrogel formulations as a function of shear rate (1/s), (F) Comparison of viscosity values of different hydrogel precursor solutions at a shear rate of 0.1 (1/s). **Solid state**: (G) Burst pressure, (H) Swelling ratio, (I) Porosity (%), (J) Compression modulus, (K) Ultimate stress, and (L) maximum strain (elasticity) of different hydrogel patch formulations after 4 min of photocrosslinking. Data are represented as mean ± SD (* $p < 0.05$, ** $p < 0.01$, ****$p < 0.0001$; n = 3).
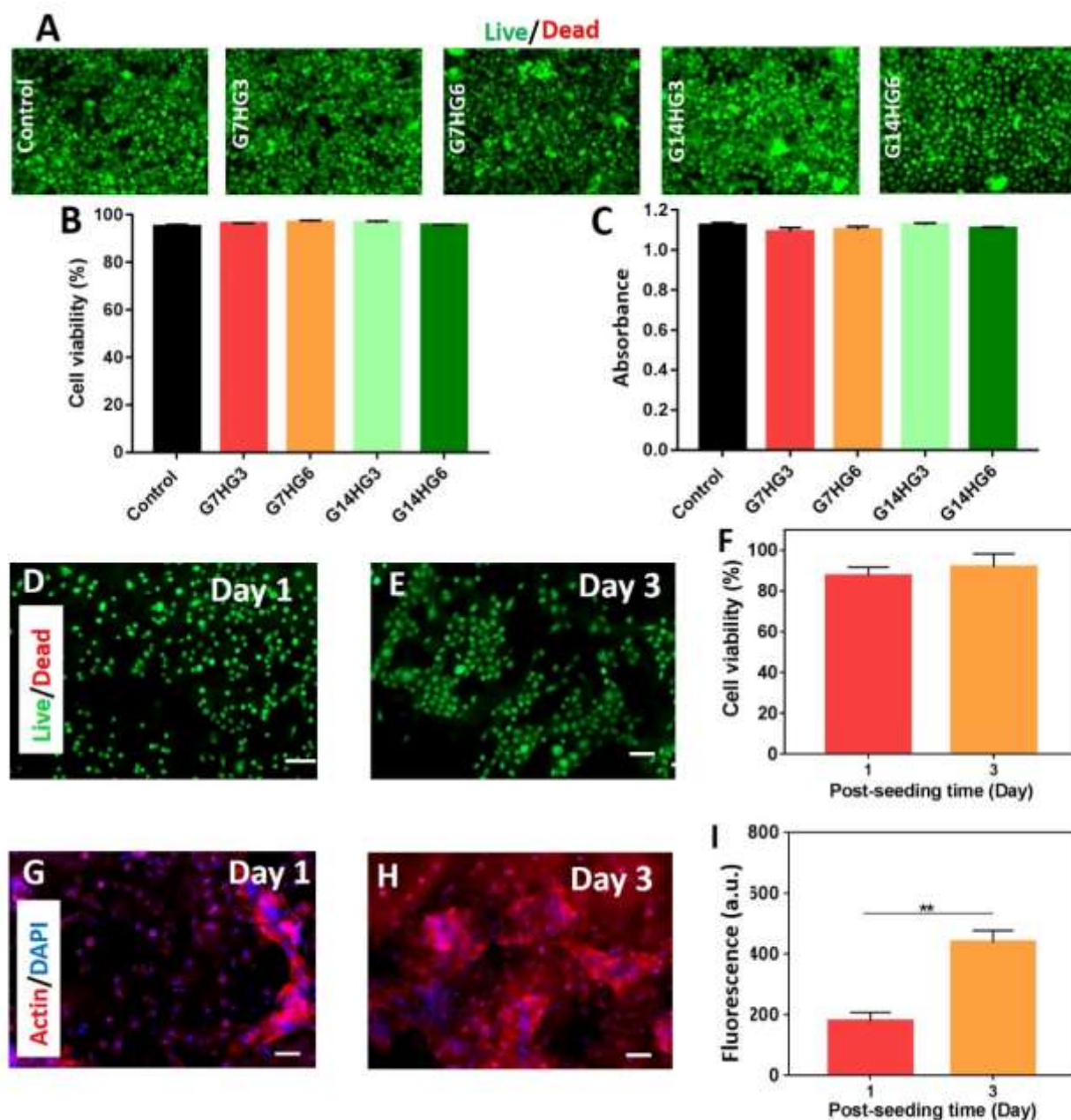
Figure 5. *In vitro* biocompatibility of the hydrogel patches. Indirect seeding: (A) Representative Live/dead stained images of human telomerase-immortalized corneal epithelial cells (hTCEpi) incubated for 24 h with culture medium or fluid extracts of photocrosslinked hydrogels prepared with different concentrations of HAGM, GelMA B300, (B) Quantification of cell viability after 24h, (C) Absorbance measured at 570 nm (690 nm background absorbance subtracted) after 24 h. **Direct seeding**: Representative LIVE/DEAD images of hTCEpi cells seeded on G7HG3 hydrogel patch on (D) day 1 and (E) day 3 (scale bar, 100 µm), (F) Quantification of cell viability after 1 and 3 days of culture, Representative Actin/DAPI images of hTCEpi cells seeded on hydrogels on (G) day 1 and (H) day 3 (scale bar, 100 µm). (I) Quantification of metabolic activity of hTCEpi cells seeded on GelPatch after 1 and 3 days. Data are represented as means ± SD (**p <0.05, n = 3).

Ins7HA3), showed burst pressure of 7.2 ± 2.3 kPa. The formulation composed of 7% (w/v) GelMA B225 and 3% (w/v) HAGM (abbreviated as Ins7HG3) showed lower burst pressure of 18.03 ± 1.4 kPa **(Fig. S12A)**.

The swelling ratio results showed the highest swelling ratio of 42.8 ± 5.3 % for the Ins7HG3 formulation. The lowest value obtained for swelling ratio was -7.1 ± 1.3 % for P1HA3 **(Fig.**

S12B). As shown previously, the addition of HAMA to the hydrogel formulation caused shrinkage. The obtained swelling ratio value for G7HG3 was 14.8 ± 3.6 % and this value decreased to -2.2 ± 0.5 % for the Ins7HA3 formulation. Taken together, based on the predefined selection criteria presented in **Table 1**, the G7HG3 hydrogel formulation best fits the required criteria.

Based on the results obtained from the previous section, among all the formulations, the hydrogel patch composed of two main components of GelMA B300 and HAGM showed results that fit well within all predefined inclusion criteria provided in **Table 1**. In our previous design space, the total polymer concentration was kept below 10% (w/v) for all combinations. Here, we studied the effect of increasing total polymer concentration on the hydrogels' properties **(Table S3)**. With this approach, we minimized the applied sample size at the initial phase of the study and specifically screened the effect of two main polymer ratios with varying total concentrations at both liquid and solid states.

Liquid state characterization

It has been previously shown that phase separation can occur for hydrogel systems composed of polymers with different physicochemical properties[36-38]. GelMA is an amphiphilic polymer composed of hydrophobic and hydrophilic moieties. On the other hand, HAGM is a highly hydrophilic polysaccharide which can form an aqueous polymer/polymer binary phase in combination with GelMA which is similar to that described for PEG and dextran[39]. In general, the miscibility of two polymers in water is governed by the following equation: $\Delta G_{mix} = \Delta H_{mix} - T\Delta S_{mix}$ where ΔG_{mix} is the free energy of mixing, ΔH_{mix} is the enthalpy of mixing, T is the absolute temperature, and ΔS_{mix} is the entropy of mixing. Phase separation occurs when ΔG_{mix} is positive, which is when $\Delta H_{mix} > 0$ and $>$ than $T\Delta S_{mix}$. For polymeric mixtures in water, it has been found that ΔS_{mix} is typically very low, and thus even small positive values of ΔH_{mix} can result in a positive ΔG_{mix} value[38].

Visual inspections combined with bright field microscopic images for all formulations composed of different weight ratios of GelMA B300 to HAGM showed aqueous phase separation **(Fig. 4A-D)**. To this end, we hypothesized that phase separation in our polymeric hydrogel system was mainly attributed to the formation and co-existence of the polymer-rich regions composed of partially dehydrated and interconnected GelMA B300, as the continuous phase, and the water-rich regions mainly composed of highly hydrated HAGM portions, as the dispersed phase.

Hydrogel formulations composed of different weight ratios of GelMA B300 to HAGM were prepared and characterized using a rheometer to check the viscosity of the hydrogel solutions in relation to their phase behavior. The obtained results showed that the hydrogel formulation formed based on 7% GelMA B300 and 3% HAGM (G7HG3) had a viscosity of 23 ± 2.5 Pa.s. The hydrogel formulation with an increase in HAGM concentration (G7HG6) showed a ~5-fold increase in viscosity (115± 6.9 Pa. s). Viscosities of 743 ± 11.6 Pa. s and 1337± 21.0 Pa. s were measured for G14HG3 and G14HG6 formulations, respectively **(Fig. 4E-F)**. According to our predefined criteria, the optimal formulation should have a viscosity value above 10 Pa. s and below 50 Pa. s to enable accommodation of the ocular surface curvature without run off or becoming diluted by tear fluid during the process of crosslinking, allowing the

formulation to be injectable. Therefore, based on the liquid state characterization, among all formulations, G7HG3 provided optimal viscosity as defined in **Table 1**. The obtained viscosity values for the GelPatch candidates were higher than the reported values for Fibrin glue and ReSure®[13,15]. This is very important characteristic since it improves the tissue retention of hydrogel prepolymer prior to photocrosslinking and prevents its run over or dilution by existing biologic liquids.

Solid state characterization

One of the predefined characteristics for the crosslinked GelPatch formulation was a burst pressure above 20 kPa. Among all formulations, only G14HG6 showed a near 2-fold increase in burst pressure (44.3 ± 7.3 kPa) as compared to G7HG3 (26.5 ± 2.8 kPa) and other formulations (G7HG6 and G14HG3) **(Fig. 4G)**. G7HG6 formulation had a burst pressure of 25.5 ± 3.5 kPa and G14HG3 had a burst pressure of 28.9 ± 1.7. However, no significant difference in burst pressure was found among G7HG3, G7HG6, and G14HG3. As explained previously, adhesion to the tissue is due to the various chemical and physical bond formations within the hydrogel itself and at the hydrogel/tissue interface **(Fig. 1B-C)**. Therefore, we hypothesized that an increase in polymer concentration would directly correlate with an increase in the number of functional groups and chemical bonds formed at the interface with the tissue. Moreover, based on the response surface analysis, there was a linear correlation between GelMA B300 and HAGM concentrations and burst pressure **(Fig. 3)**. However, the results showed that there are other existing parameters such as stiffness and shape accommodation properties of the crosslinked hydrogel which can counter affect the surface adhesion properties of the developed hydrogel patch. Direct correlation between increased adhesion with increased polymer concentration was only observed at a GelMA B300/HAGM weight ratio of 2.33 **(Table S3)**. The overall obtained results for burst pressure of GelPatch formulations showed higher values compared to the results obtained from the previous study where the maximum bust pressure of 19.7±7.3 kPa was reported for the for the G7HG3 candidate [15]. This value was reported to be 15.4 ± 6.3 kPa for the commercial product, ReSure®[9, 10]. Burst pressure value reported for GelCORE hydrogel was ~58 to 63 kPa, however, the applied total polymer concentration was at 20% (w/v)[13].

Swelling ratio is another important parameter which can impact the adhesive properties of the hydrogel patch to biologic surfaces over time. Adhesive hydrogels with a high swelling ratio tend to deform fast, cause discomfort, and detach from the ocular surface. Therefore, the inclusion criteria for swelling ratios for our optimized hydrogel patch was chosen to be ≤ 20%. Based on the statistical analysis, PEGDA and HAGM were identified as the two main factors which enhanced the swelling ratio **(Table 2)**. The swelling ratios for G7HG3 and G7HG6 were 14.2 ± 2.1% and 25.4± 3.5%, respectively. The swelling ratios for G14HG3 and

G14HG6 were 5.8 ± 1.5% and 15.3 ± 2.9%, respectively **(Fig. 4H)**. The results indicate that an increase in GelMA B300 concentration caused a decrease in the amount of water absorbed and, therefore, decreased the swelling ratio. This was most likely due to an increase in crosslinking density of the hydrogel which repelled the water molecules[40]. However, the addition of a highly hydrophilic polysaccharide such as HAGM, with a high molecular weight, enhanced water bonding capacity. This combined with its lower degree of methacrylation (~12%) compared to GelMA B300, caused an increase in overall swelling properties of the crosslinked hydrogel. There is a direct correlation between an increase in HAGM content and swelling ratio of the hydrogel. The optimum GelPatch formulations with the desired swelling ratios were G7HG3 and G14HG3 with swelling ratios of 14.2 ± 2.1% and 5.8 ± 1.5%, respectively **(Fig. 4H)**, based on predefined inclusion criteria. Comparing our results with previous studies, the overall reported swelling ratio values from current study was lower compared to the swelling ratio of 30 ± 3% reported for selected hydrogel patch(G4P1H3) from the previous study[15] which was composed of small molecular weight porcine GelMA, PEGDA, and HAGM. This difference in swelling ratio can be primarily due to the difference in degree of modifications of the applied polymers and presence of PEGDA within the Hydrogel composition.

Another important parameter in the design of the hydrogel patch for ocular application is their porosity. Previously, it was shown that creating a porous network with porosity within the range of 30-40% can facilitate diffusion of necessary nutrients, gas exchanges, and 3D cell and tissue growth within the hydrogel scaffold[40-42]. The obtained values for porosity of GelPatch candidates, showed a decrease in porosity percentage with an increase in total polymer concentration. G7HG3 showed a porosity of 34.1 ± 0.42%; however, the formulation containing the highest polymer concentration, G14HG6, showed a porosity of 23.7 ± 1.44% **(Fig. 4I)**. In general, porosity can be considered one of the desired characteristics of the hydrogel patch in order to provide water and oxygen to the (tissue) contact area. Also, it is important for providing enough void volume for tissue ingrowth once a hydrogel patch is applied on injured tissues. However, it is important to note that an increase in porosity (~80-90%) can also inversely impact the burst pressure and the mechanical properties of the hydrogel patch due to an increase in density of interconnected pores.

In addition to the above properties, an ideal ocular patch should be also flexible and non-rigid in order to accommodate the shape of the eye upon crosslinking on the surface. Experimental results of the formulated patches showed that an increase in overall polymer concentration enhanced the compression modulus. For example, the compression modulus was 14.68 ± 1.5 kPa for G7HG3 and 40.50 ± 4.5 kPa for G14HG6. The compression modulus for G7HG6 and G14HG3 was 26.22 ± 1.9 and 32.20 ± 5.60 kPa, respectively **(Fig. 4J)**. The ultimate stress was 813.8 ± 115 kPa for G7HG3

and 1,534 ± 382 kPa for G14HG6, respectively. The ultimate stress for G7HG6 and G14HG3 was 1,047 ± 169 and 1,327.8 ± 227 kPa, respectively **(Fig. 4K)**. In addition, an increase in the compressive modulus of the hydrogel patches did not compromise the elasticity. All formulations showed an elasticity (i.e., maximum strain) of ~75% **(Fig. 4L)**. The overall results suggest that among all the hydrogel patch formulations, G7HG3 is the most desirable formulation.

In vitro degradation of the optimized GelPatch formulation

One advantage of using naturally derived hydrogels for biomedical applications is their degradation in wet environments without producing toxic by-products. Controlling the degradation rate of the hydrogel in the presence of enzymes is important, since it gives the possibility to precisely fine tune the degradation rate of adhesive patches based on the wound healing process. So far, studies have shown that ocular irritation and inflammation can induce endogenous and exogenous secretion of enzymes such as collagenase and hyaluronidase[43-48]. The concentrations of secreted enzymes have been reported to vary based on the intensity and type of ocular damages[45, 46]. In this study, degradation study was carried out in the presence of two enzymes: collagenase type II and hyaluronidase. To mimic different natural ocular conditions from severe to mild inflammation, various concentrations of both enzymes including 0.5, 2.0, 5.0, 10.0 and 20.0 (μg/mL) were used to evaluate the degradation rate of the optimized GelPatch formulation G7HG3 **(Fig. S13)**. The data showed that an increase in both enzyme concentrations enhanced the degradation rate. At the dual enzyme concentration of 0.5 (μg/mL) only 10.7 ± 1.8% of the patch degraded within the time period of 5 days. However, this value increased to 55.1 ± 2.1% for 5.0 (μg/mL) dual enzyme concentrations. Finally, full degradation of the hydrogel was observed at the maximum dual enzyme concentrations of 20 (μg/mL) after 3 days.

In vitro biocompatibility of GelPatch

To evaluate the biocompatibility of the GelPatch, cellular viability and metabolic activity assays were performed using hTCEpi based on two methods: indirect seeding and direct seeding **(Fig. 5)**. For indirect seeding, different formulations of hydrogel incubated fluid extracts were applied to a confluent hTCEpi monolayer. The cells were investigated through Live/Dead assay and PrestoBlue assay after 1 day of incubation at 37°C. The micrographs of stained cells by Live/Dead assay showed a high viability of cells (>97%) for all tested hydrogels **(Fig. 5A-B)**. The results also demonstrated that there was no significant difference in cell viability between different hydrogel formulations. In addition, PrestoBlue assay showed no significant difference in absorbance when measured between all groups tested **(Fig. 5C)**. These results suggest that the hydrogel formulations were not toxic.

Biomaterials Science

For direct seeding, hTCEpi cells were seeded on the surface of the selected crosslinked G7HG3 patch formulation and cell viability, spreading, and proliferation were assessed on days 1 and 3. The micrographs of stained cells by Live/Dead assay at days 1 and 3 showed high viability of cells (>90%) seeded on samples at the early stage of their culture **(Fig. 5D-F)**. In addition, the morphology of the cultured cells on the hydrogels was evaluated using fluorescent staining F-actin in the cytoskeleton of cells on days 1 and 3. The assembly of F-actin cytoskeleton of cells in fluorescent micrographs showed that the cells spread, adhered, and proliferated on the surface of the G7HG3 GelPatch, indicating the *in vitro* biocompatibility of the samples for cell adherence and growth **(Fig. 5G-H)**. The metabolic activity of cultured hTCEpi cells on samples were assessed through PrestoBlue assay

and showed a consistent increase (P < 0.05) over 3 days, confirming the biocompatibility of the hydrogel formulation **(Fig. 5I)**.

Ex vivo assessment of GelPatch hydrogel adhesion to the Cornea, sclera and subconjunctival space

The hydrogel formulation of G7HG3 was selected as the optimized hydrogel patch formulation based on previous experiments. Therefore, the adhesion and retention of G7HG3 hydrogel patch was studied using an *ex vivo* rabbit eye model as described previously. First the ability of the hydrogel formulation to withstand bursting when applied onto a linear full-thickness laceration was evaluated **(Fig. 6A)**. The results demonstrated a scleral burst pressure of 31.22 ± 7.77 kPa, and a corneal burst pressure of 4.9 ± 2.00
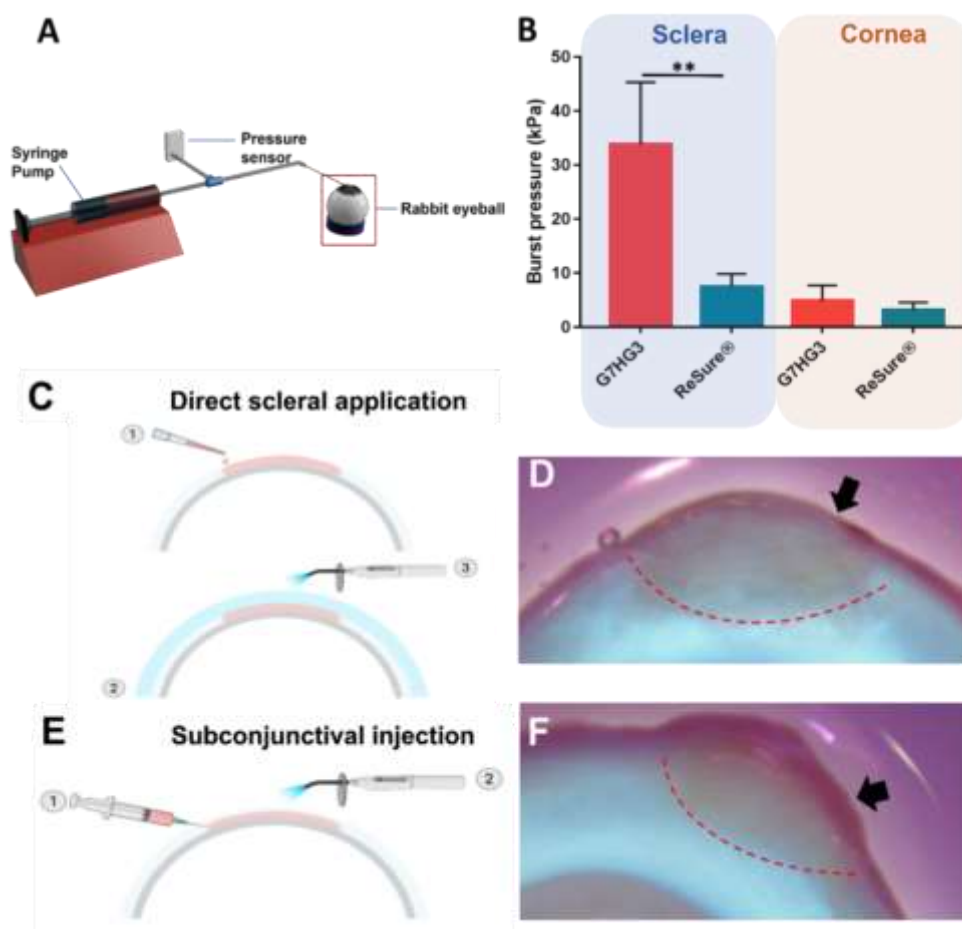

Figure 6. *Ex vivo* adhesion and retention assessment of GelPatch using rabbit eyeball. (A) Schematic of *ex vivo* burst pressure setup connected via a needle to the aqueous humor of the eyeball and the pressure sensor. (B) Average burst pressure of G7HG3 GelPatch formulation and commercially available sealant ReSure®, applied on the surface of sclera and/or cornea. (C) Schematic of the GelPatch application process to the sclera by (1) direct application onto the sclera and (2) overlay of a contact lens prior to (3) crosslinking of the bioadhesive. (D) GelPatch formulations at day 0 following crosslinking after direct scleral application of the G7HG3 formulation (E) Schematic of subconjunctival injection of the GelPatch application process to the subconjunctival space by (1) subconjunctival injection and (2) crosslinking on top of the overlying conjunctiva. (F) GelPatch formulations at day 0 following crosslinking after subconjunctival injection of G7HG3 formulation. (Graphics were created using BioRender.com). Data is represented as mean ± SD (* p < 0.05, ** p< 0.01, ****p < 0.0001; n > 4).

ARTICLE

kPa. The formulation was compared to ReSure® sealant which showed a scleral burst pressure of 10.8 ± 3.47 kPa, and corneal burst pressure of 2.84± 1.1 kPa **(Fig. 6B)**. These findings suggest that the optimized GelPatch could withstand a larger amount of pressure compared to current standards of commercially available hydrogel sealants.

Next, G7HG3 formulation was applied either directly on the sclera or via subconjunctival injection route **(Fig. 6C-E)**. Each day, the adhesion and retention of the bioadhesives to the sclera and subconjunctiva were assessed for up to 4 days. The patch showed continuous adhesion to the sclera **(Fig. 6D)** and subconjunctival space **(Fig. 6F)** up to 4 days**.** No visible signs of reduced adhesion were observed at the ending time point of 4 days. The chosen method of testing adhesion was limited due to non-quantifiable differences in applied force used for each sample. However, the hydrogel was able to withstand a great amount of mechanical manipulation without noticeably affecting adhesive strength. For scleral application of G7HG3, see **movie S1** and for subconjunctival injected G7HG3 hydrogel patch see **movie S2**.

Conclusion

In this study, we used polymers with different levels of methacrylation, molecular weights, and hydrophobic /hydrophilic properties to engineer highly adhesive patches for ocular applications. A series of patches were formulated and characterized based on high wet tissue (ocular) retention upon instillation, ocular adhesion, swelling, strength, and elasticity. A DSD model was used to screen the effects of the polymers on response parameters, to select the most prominent (significant) polymer on each response parameter, and to check for non-linearity of correlations (two-way interactions) among the polymers.

Based on previously performed studies by our group, we defined new selection criterion for optimizing GelPatch formulation which can be applicable for ocular sealing. Two types of modified hyaluronic acid polymers were applied in this study to improve the ocular retention and the initial viscosity of the hydrogel patch. Two types of methacrylated porcine gelatin polymers were applied as the main

components for tissue adhesion. PEGDA was used to screen for a possible synergic effect with other polymers in the formulation and improved properties.

In our study, we showed that GelMA 300 and HAGM had a main impact on burst pressure. Although HAGM itself significantly increased swelling of the GelPatch, its combination with GelMA B300 balanced out the high swelling properties, decreased the stiffness, and improved elasticity compared to other formulations. PEGDA was found to have no significant impact on burst pressure nor on swelling at the applied concentration ranges. HAMA was a highly desirable polymer candidate to minimize the swelling ratio and to improve the overall strength and stiffness of the crosslinked hydrogel. However, its addition to the GelPatch caused an excessive increase in viscosity which failed our predefined selection criteria for initial viscosity. Therefore, among five applied polymers, only two polymers (GelMA B300 and HAGM) were selected to be applied as GelPatch formulation of G7HG3. The optimized GelPatch candidate showed high *in vitro* biocompatibility. The *ex vivo* results on subconjunctival and scleral application of the candidate GelPatch formulation (G7HG3), showed high adhesion and resistance after 4 days of incubation in an organ bath. Our findings suggest that GelPatch adhesion and retention on the ocular surface could be utilized as a sealant for ocular injuries (incisions). Further investigation is necessary in *ex vivo* and *in vivo* models to further evaluate the functionality of our designed patch.

Conflicts of interest

N.A. and R.D. hold equity in GelMEDIX Inc.

Acknowledgments

References

1. J. P. Whitcher, M. Srinivasan and M. P. Upadhyay, *Bull World Health Organ*, 2001, 79, 214-221.
2. R. R. A. Bourne, S. R. Flaxman, T. Braithwaite, M. V. Cicinelli, A. Das, J. B. Jonas, J. Keeffe, J. H. Kempen, J. Leasher, H. Limburg, K. Naidoo, K. Pesudovs, S. Resnikoff, A. Silvester, G. A. Stevens, N. Tahhan, T. Y. Wong and H. R. Taylor, *Lancet Glob Health*, 2017, 5, e888-e897.
3. G. Y. Kong, R. H. Henderson, S. S. Sandhu, R. W. Essex, P. J. Allen and W. G. Campbell, *Clinical & Experimental Ophthalmology*, 2015, 43, 508-513.
4. V. Jhanji, A. L. Young, J. S. Mehta, N. Sharma, T. Agarwal and R. B. Vajpayee, *Survey of Ophthalmology*, 2011, 56, 522-538.
5. D. J. Pieramici, M. W. MacCumber, M. U. Humayun, M. J. Marsh and E. de Juan, *Ophthalmology*, 1996, 103, 1798-1803.
6. C. E. Hugkulstone, *J R Soc Med*, 1992, 85, 322-323.
7. C. D. McTiernan, F. C. Simpson, M. Haagdorens, C. Samarawickrama, D. Hunter, O. Buznyk, P. Fagerholm, M. K. Ljunggren, P. Lewis, I. Pintelon, D. Olsen, E. Edin, M. Groleau, B. D. Allan and M. Griffith, *Sci Adv*, 2020, 6.
8. S. Guhan, S. L. Peng, H. Janbatian, S. Saadeh, S. Greenstein, F. Al Bahrani, A. Fadlallah, T. C. Yeh and S. A. Melki, *Br J Ophthalmol*, 2018, 102, 1328-1335.

9. D. Li, J. Chen, X. Wang, M. Zhang, C. Li and J. Zhou, *Frontiers in Bioengineering and Biotechnology*, 2020, 8.

10. S. Hoshi, F. Okamoto, M. Arai, T. Hirose, Y. Sugiura, Y. Kaji and T. Oshika, *Investigative Ophthalmology & Visual Science*, 2015, 56, 4705-4711.

11. L. Sanders and J. Nagatomi, *Crit Rev Biomed Eng*, 2014, 42, 271-292.

12. D. H. Sierra, *Journal of Biomaterials Applications*, 1993, 7, 309-352.

13. E. S. Sani, A. Kheirkhah, D. Rana, Z. Sun, W. Foulsham, A. Sheikhi, A. Khademhosseini, R. Dana and N. Annabi, *Science Advances*, 2019, 5, eaav1281.

14. W. D. Spotnitz, *ISRN Surgery*, 2014, 2014, 203943.

15. C. Jumelle, A. Yung, E. S. Sani, Y. Taketani, F. Gantin, L. Bourel, S. Wang, E. Yüksel, S. Seneca, N. Annabi and R. Dana, *Acta Biomaterialia*, 2022, 137, 53-63.

16. N. Annabi, Y. N. Zhang, A. Assmann, E. S. Sani, G. Cheng, A. D. Lassaletta, A. Vegh, B. Dehghani, G. U. Ruiz-Esparza, X. Wang, S. Gangadharan, A. S. Weiss and A. Khademhosseini, *Sci Transl Med*, 2017, 9.

17. F. Tan, X. Xu, T. Deng, M. Yin, X. Zhang and J. Wang, *Biomed Mater*, 2012, 7, 055009.

18. E. Hachet, H. Van Den Berghe, E. Bayma, M. R. Block and R. Auzély-Velty, *Biomacromolecules*, 2012, 13, 1818-1827.

19. B. S. Spearman, N. K. Agrawal, A. Rubiano, C. S. Simmons, S. Mobini and C. E. Schmidt, *J Biomed Mater Res A*, 2020, 108, 279-291.

20. E. Hoch, C. Schuh, T. Hirth, G. E. M. Tovar and K. Borchers, *Journal of Materials Science: Materials in Medicine*, 2012, 23, 2607-2617.

21. N. Naseri, B. Deepa, A. P. Mathew, K. Oksman and L. Girandon, *Biomacromolecules*, 2016, 17, 3714-3723.

22. S. Sultan and A. P. Mathew, *Nanoscale*, 2018, 10, 4421-4431.

23. R. Kenett, Sh. Zacks and D. Amberti, *Modern Industrial Statistics: with applications in R, MINITAB and JMP*, 2nd edn., 2014.

24. A. Erler, N. de Mas, P. Ramsey and G. Henderson, *Biotechnology Letters*, 2013, 35, 323-329.

25. C.-Y. Lin and P. Yang, *Journal of Quality Technology*, 2015, 47, 351-362.

26. M. Ghovvati, S. Baghdasarian, A. Baidya, J. Dhal and N. Annabi, *Journal of Biomedical Materials Research Part B: Applied Biomaterials*, 2022, 110, 1511-1522.

27. S. Baghdasarian, B. Saleh, A. Baidya, H. Kim, M. Ghovvati, E. S. Sani, R. Haghniaz, S. Madhu, M. Kanelli, I. Noshadi and N. Annabi, *Materials Today Bio*, 2022, 13, 100199.

28. J. Moreira, A. C. Vale and N. M. Alves, *Journal of Materials Chemistry B*, 2021, 9, 3778-3799.

29. G. Zhao, S. Kaur and T. Wang, *Organic Letters*, 2017, 19, 3291-3294.

30. J. Yang, R. Bai, J. Li, C. Yang, X. Yao, Q. Liu, J. J. Vlassak, D. J. Mooney and Z. Suo, *ACS Applied Materials & Interfaces*, 2019, 11, 24802-24811.

31. L. Gong, L. Xiang, J. Zhang, J. Chen and H. Zeng, *Langmuir*, 2019, 35, 15914-15936.

32. Y. Zhou, S. Li, D. Wang, Y. Zhao and X. Lei, *Bioscience Journal*, 2018, 34, 778-789.

33. A. J. Miles and B. A. Wallace, *Chemical Society Reviews*, 2006, 35, 39-51.

34. J. Liu and J. Song, *Biophys J*, 2008, 95, 4803-4812.

35. V. N. Uversky, *Protein Sci*, 2002, 11, 739-756.

36. J. Gong, C. C. L. Schuurmans, A. M. v. Genderen, X. Cao, W. Li, F. Cheng, J. J. He, A. López, V. Huerta, J. Manríquez, R. Li, H. Li, C. Delavaux, S. Sebastian, P. E. Capendale, H. Wang, J. Xie, M. Yu, R. Masereeuw, T. Vermonden and Y. S. Zhang, *Nature Communications*, 2020, 11, 1267.

37. A. N. Semenov, J. F. Joanny and A. R. Khokhlov, *Macromolecules*, 1995, 28, 1066-1075.

38. J. Sprakel, N. A. M. Besseling, M. A. Cohen Stuart and F. A. M. Leermakers, *Eur. Phys. J. E*, 2008, 25, 163-173.

39. P.-Å. Albertsson, in *Advances in Protein Chemistry*, eds. C. B. Anfinsen, J. T. Edsall and F. M. Richards, Academic Press, 1970, vol. 24, pp. 309-341.

40. R. J. Stenekes, O. Franssen, E. M. van Bommel, D. J. Crommelin and W. E. Hennink, *Pharm Res*, 1998, 15, 557-561.

41. X. Hu, L. Ma, C. Wang and C. Gao, *Macromolecular Bioscience*, 2009, 9, 1194-1201.

42. K. W. M. Boere, M. M. Blokzijl, J. Visser, J. E. A. Linssen, J. Malda, W. E. Hennink and T. Vermonden, *Journal of Materials Chemistry B*, 2015, 3, 9067-9078.

43. F. P. W. Melchels, W. J. A. Dhert, D. W. Hutmacher and J. Malda, *Journal of Materials Chemistry B*, 2014, 2, 2282-2289.

44. S. J. Hollister, *Nat Mater*, 2005, 4, 518-524.

45. E. D. Conway, Master of Science, Purdue University, 2015.

46. C. B. Ibberson, DOI: 10.17077/etd.uyknxveb, University of Iowa, 2015.

47. G. Mayer, I. C. Michaelson and N. Herz, *Br J Ophthalmol*, 1956, 40, 53-56.

48. E. Payan, J. Y. Jouzeau, F. Lapicque, N. Muller and P. Netter, *International Journal of Biochemistry*, 1993, 25, 325-329.